Research Article | Vol. 24, No. 24 | 28 Nov 2016 | OPTICS EXPRESS 28104

Optics EXPRESS

Surface modulation and back reflection from foil targets irradiated by a Petawatt femtosecond laser pulse at oblique incidence

S. TER-AVETISYAN,[1,2,*] A. ANDREEV,[3,4,5] K. PLATONOV,[6] J. H. SUNG,[7] S. K. LEE,[7] H. W. LEE,[1] J. Y. YOO,[1] P. K. SINGH,[1] H. AHMED,[8] C. SCULLION,[8] K. F. KAKOLEE,[1] T. W. JEONG,[1,2] P. HADJISOLOMOU,[8] AND M. BORGHESI[8]

[1]*Center for Relativistic Laser Science, Institute of Basic Science (IBS), Gwangju 61005, South Korea*
[2]*Department of Physics and Photon Science, Gwangju Institute of Science and Technology (GIST), Gwangju 61005, South Korea*
[3]*Max-Born-Institute, Berlin D-12489, Germany*
[4]*ELI-ALPS, Szeged H-6720, Hungary*
[5]*St. Petersburg University IFMO, St. Petersburg 196135, Russia*
[6]*Vavilov State Optical Institute, St. Petersburg 199064, Russia*
[7]*Ultra-intense Laser Laboratory, Advanced Photonics Research Institute, Gwangju Institute of Science and Technology (GIST), Gwangju 61005, South Korea*
[8]*School of Mathematics and Physics, The Queen's University of Belfast, Belfast, BT7 1NN, UK*
[*]*sargis@gist.ac.kr*

Abstract: A significant level of back reflected laser energy was measured during the interaction of ultra-short, high contrast PW laser pulses with solid targets at 30° incidence. 2D PIC simulations carried out for the experimental conditions show that at the laser-target interface a dynamic regular structure is generated during the interaction, which acts as a grating (quasi-grating) and reflects back a significant amount of incident laser energy. With increasing laser intensity above 10^{18} W/cm^2 the back reflected fraction increases due to the growth of the surface modulation to larger amplitudes. Above 10^{20} W/cm^2 this increase results in the partial destruction of the quasi-grating structure and, hence, in the saturation of the back reflection efficiency. The PIC simulation results are in good agreement with the experimental findings, and, additionally, demonstrate that in presence of a small amount of pre-plasma this regular structure will be smeared out and the back reflection reduced.

OCIS codes: (240.6648) Surface dynamics, (260.7120) Ultrafast phenomena, (350.5400) Plasmas, (140.7090) Ultrafast lasers.

References and links

1. A. Macchi, M. Borghesi, and M. Passoni, "Ion acceleration by superintense laser-plasma interaction," Rev. Mod. Phys. **85**(2), 751–793 (2013).
2. J. R. Davies, "Laser absorption by overdense plasmas in the relativistic regime," Plasma Phys. Contr. Fusion **51**(1), 014006 (2009).
3. B. Dromey, S. Kar, C. Bellei, D. C. Carroll, R. J. Clarke, J. S. Green, S. Kneip, K. Markey, S. R. Nagel, P. T. Simpson, L. Willingale, P. McKenna, D. Neely, Z. Najmudin, K. Krushelnick, P. A. Norreys, and M. Zepf, "Bright multi-keV harmonic generation from relativistically oscillating plasma surfaces," Phys. Rev. Lett. **99**(8), 085001 (2007).
4. A. Andreev, V. M. Komarov, A. V. Charukhchev, and K. Yu. Platonov, "Backscattering of a high-intensity ultrashort laser pulse from a solid target at oblique incidence," Opt. Spectrosc. **102**(6), 944–948 (2007).
5. A. Andreev, K. Platonov, and R. R. E. Salomaa, "Backscattering of ultrashort high intensity laser pulses from solid targets at oblique incidence," Phys. Plasmas **9**(2), 581–588 (2002).
6. S. C. Wilks, W. L. Kruer, M. Tabak, and A. B. Langdon, "Absorption of ultra-intense laser pulses," Phys. Rev. Lett. **69**(9), 1383–1386 (1992).
7. M. Zepf, M. Castro-Colin, D. Chambers, S. G. Preston, J. S. Wark, J. Zhang, C. N. Danson, D. Neely, P. A. Norreys, A. E. Dangor, A. Dyson, P. Lee, A. P. Fews, P. Gibbon, S. Moustaizis, and M. H. Key, "Measurements

#275721 http://dx.doi.org/10.1364/OE.24.028104
Journal © 2016 Received 30 Sep 2016; revised 13 Nov 2016; accepted 14 Nov 2016; published 23 Nov 2016

Optics EXPRESS

of the hole boring velocity from Doppler shifted harmonic emission from solid targets," Phys. Plasmas **3**(9), 3242–3244 (1996).
8. B. Dromey, D. Adams, R. Hörlein, Y. Nomura, S. G. Rykovanov, D. C. Carroll, P. S. Foster, S. Kar, K. Markey, P. McKenna, D. Neely, M. Geissler, G. D. Tsakiris, and M. Zepf, "Diffraction-limited performance and focusing of high harmonics from relativistic plasmas," Nat. Phys. **5**(2), 146–152 (2009).
9. M. Yeung, B. Dromey, D. Adams, S. Cousens, R. Hörlein, Y. Nomura, G. D. Tsakiris, and M. Zepf, "Beaming of high-order harmonics generated from laser-plasma interactions," Phys. Rev. Lett. **110**(16), 165002 (2013).
10. H. Vincenti, H. Vincenti, S. Monchocé, S. Kahaly, G. Bonnaud, Ph. Martin and F. Quéré, "Optical properties of relativistic plasma mirrors," Nat. Commun. **5**, 3403 (2014).
11. S. Eliezer, *The Interaction Of High-Power Lasers With Plasmas* (IoP Publishing Ltd 2002).
12. T. J. Yu, S. K. Lee, J. H. Sung, J. W. Yoon, T. M. Jeong, and J. Lee, "Generation of high-contrast, 30 fs, 1.5 PW laser pulses from chirped-pulse amplification Ti:sapphire laser," Opt. Express **20**(10), 10807–10815 (2012).
13. J. H. Sung, S. K. Lee, T. M. Jeong, and C. H. Nam, "Enhancement of temporal contrast of high-power femtosecond laser pulses using two saturable absorbers in the picosecond regime," Appl. Phys. B **116**(2), 287–292 (2014).
14. P. K. Singh, K. F. Kakolee, T. W. Jeong, and S. Ter-Avetisyan, "A diagnostic for micrometer sensitive positioning of solid targets in intense laser-matter interaction," Nucl. Instrum. Meth. A **829**, 363–366 (2016).
15. T. W. Jeong, P. K. Singh, C. Scullion, H. Ahmed, K. F. Kakolee, P. Hadjisolomou, A. Alejo, S. Kar, M. Borghesi, and S. Ter-Avetisyan, "Experimental evaluation of the response of micro-channel plate detector to ions with 10s of MeV energies," Rev. Sci. Instrum. **87**(8), 083301 (2016).
16. V. Yu. Bychenkov, P. K. Singh, H. Ahmed, K. F. Kakolee, C. Scullion, T. W. Jeong, P. Hadjisolomou, A. Alejo, S. Kar, M. Borghesi, and S. Ter-Avetisyan, "Ion acceleration in the electrostatic field of charged cavity created by relativistic ultra-short laser pulses of 10^{20}-10^{21} W/cm²," Phys. Plasmas. submitted.
17. M. Schnürer, S. Ter-Avetisyan, S. Busch, E. Risse, M. P. Kalachnikov, M. Sandner, and P. V. Nickles, "Ion acceleration with ultrafast laser driven water droplets," Laser Part. Beams **21**, 337–343 (2005).
18. A. A. Andreev, S. Steinke, T. Sokollik, M. Schnürer, S. Ter-Avetsiyan, K. Y. Platonov, and P. V. Nickles, "Optimal ion acceleration from ultrathin foils irradiated by a profiled laser pulse of relativistic intensity," Phys. Plasmas **16**(1), 013103 (2009).
19. A. Andreev and K. Platonov, "Generation of electron nanobunches and short-wavelength radiation upon reflection of a relativistic-intensity laser pulse from a finite-size target," Opt. Spectrosc. **114**(5), 788–797 (2013).
20. A. Sgattoni, S. Sinigardi, L. Fedeli, F. Pegoraro, and A. Macchi, "Laser-driven Rayleigh-Taylor instability: plasmonic effects and three-dimensional structures," Phys. Rev. E Stat. Nonlin. Soft Matter Phys. **91**(1), 013106 (2015).
21. Y. Wan, C.-H. Pai, C. J. Zhang, F. Li, Y. P. Wu, J. F. Hua, W. Lu, Y. Q. Gu, L. O. Silva, C. Joshi, and W. B. Mori, "Physical mechanism of the transverse instability in radiation pressure ion acceleration," Phys. Rev. Lett., in press (2016).
22. A. Macchi, F. Cornolti, and F. Pegoraro, "Two-surface wave decay," Phys. Plasmas **9**(5), 1704 (2002).
23. D. an der Brügge, N. Kumar, A. Pukhov, and C. Rödel, "Influence of surface waves on plasma high-order harmonic generation," Phys. Rev. Lett. **108**(12), 125002 (2012).
24. N. M. Naumova, J. A. Nees, I. V. Sokolov, B. Hou, and G. A. Mourou, "Relativistic generation of isolated attosecond pulses in a λ 3 focal volume," Phys. Rev. Lett. **92**(6), 063902 (2004).

1. Introduction

The interaction of high intensity, ultrashort laser pulses with solid targets has been studied extensively over the last decade [1]. During the interaction of high contrast, ultrashort and intense laser pulses (above 10^{18} W/cm^2) with steep plasma of solid density, laser energy is transferred to the electrons mainly via the ponderomotive mechanism [2], leading to the penetration of large electron currents into the bulk of the target. When the intense interaction takes place at a sharp plasma-vacuum boundary the electric field of the laser can cause the electrons in the plasma surface to move in phase constituting a "relativistic mirror" which oscillates at the laser frequency, leading to harmonic generation through up-shifting and compression of the laser light reflected at the critical surface [3].

Modulated structures can also be generated at the critical surface, which can reflect back an obliquely incident laser pulse, as was observed with picosecond pulses at weakly relativistic intensities (~10^{18} W/cm^2) [4]. For short laser pulses (100 fs) the back reflection was studied in [5], at relatively low pulse contrast and laser intensities (~10^{16} W/cm^2). In this case the backscattering process was attributed to scattering from a plasma wave generated within the preplasma present in front of the target surface.

At strongly relativistic laser intensities and high laser pulse contrast – i.e. in absence of any extended preplasma-back reflection may result from a different effect, i.e. the

Optics EXPRESS

deformation of the critical surface of the plasma caused by the radiation pressure of the laser pulse, through the so called “hole boring” effect [6–8]. The effects of ponderomotive denting of the critical surface have been observed on high harmonics beams, causing the dynamically varying divergence of harmonic beams from overdense plasma surfaces [9], and focusing effects in the specularly reflected radiation [10]. Furthermore, the interplay between the incident beam and the reflected light can make the overall system parametrically unstable and lead to the rapid growth of Rayleigh-Tailor type [11] instabilities. Therefore, the effects which may lead to laser light reflection from the critical density surface at the intensities nowadays available on state of the art systems (exceeding 10^{21} W/cm^2), become more complex and require special attention.

We report in this paper measurements of backscattered radiation from the interaction of obliquely incident, PW-level laser pulses with solid targets. The back scattered energy level observed is of the order of several % of the incident laser pulse energy, which can represent a concern for the safe operation of laser systems, as the reflected laser light can effectively travel back through the transport system and, if imperfectly collimated by the focusing optics, might even be focused on optical components causing serious damage. PIC simulations of the laser-solid interaction suggest that the growth of dynamic density modulations at the reflecting surface may be responsible for the observed backscattering.

2. Experimental set-up

The experiments were performed with the 1.5 petawatt, CPA laser system at the Center for Relativistic Laser Science (CoReLS), IBS [12]. A detailed schematic of the experimental set up is shown in Fig. 1. A 30 fs laser pulse was focused using an f/3 off-axis parabola on to an *Al* foil target at an angle of incidence of 30°. The temporal contrast of the laser pulse was characterized by a scanning third order cross correlator with a dynamic range of 10^{10} having a temporal resolution of 100 fs, and a scanning range of ± 650 ps. Employing a “saturable absorber” technique [13] a laser pulse temporal contrast ~5×10^{-10} was achieved at a few ps before the main pulse (see the measured contrast ratio in Fig. 6 of [12]). The pulse shape close to the peak was unchanged, and no significant pre-pulses preceding the main pulse were observed in both cases. The focal spot, measured with attenuated laser energy, contained nearly 30% of energy within the 4 μm FWHM. A target position monitoring diagnostic with a few micrometers accuracy was used to locate the target foil at the laser focus plane [14]. The laser intensity was changed by varying laser energy while the interaction geometry was kept constant.

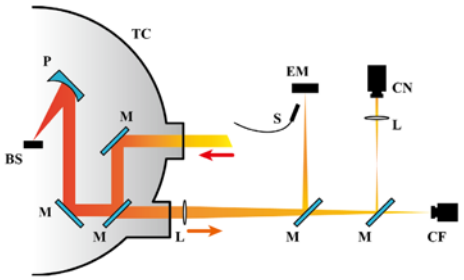

Fig. 1. Sketch of experimental setup. Acronyms used in the sketch are: TC- target chamber, P- parabolic mirror M- mirror, BS- back-reflection source, L- lens, EM- energy meter, S- spectrometer, CN- near-field measurement camera, CF- far-field measurement camera.

Two absolutely calibrated Thomson parabola spectrometers [15] were employed to record the energy spectra of accelerated ions along the rear and front surface target normal directions. The observed continuous proton energy increase from both sides of the target with increasing laser intensity from 0.2 × 10^{21} W/cm^2 up to 1.2 × 10^{21} W/cm^2 at target thicknesses 6, 2, 1.5, 0.4, 0.2 and 0.1 μm [16] indicates that the mechanism of ion acceleration in this

Optics EXPRESS

large intensity range stays unchanged. Otherwise brake-up [17], or some discontinuity in proton cutoff energy increase with increasing laser intensity could be measured. Therefore one can argue that there is no effect which can be attributed to the change of laser interaction conditions while increasing laser intensity including the significance of the laser pulse contrast at high intensities.

Back reflected laser radiation was taken from the transmission leakage of one of the turning mirrors and transported out of the chamber. The back-reflection source was relayed using a Keplerian telescope with magnification 200:3. The near field image was reconstructed at 2.49 cm after the second lens. Inside the telescope a 50:50 beam-splitter was inserted to measure the pulse energy (with a PE10 Ophir energy meter) and spectrum (using a HR4000, Ocean Optics). A second beam-splitter divided the beam into near-field and far-field monitoring CCD cameras.

The energy calibration of the measuring system was performed by placing an *Al* mirror before the off-axis parabola to reflect back the beam. Measured laser energy inside and outside the chamber was averaged over 100 shots and the calibration factor of 632.7 was deduced. The back reflected laser light was controlled also in the laser chain using a photodiode installed after the pre-amplifier and the first amplifier [12] which showed one-to-one correlation with the measurements outside the chamber in our setup. To confirm that the measured signal is a reflection from the target and not from optical elements inside the chamber or along the beam path, test shots were performed without target in place. No signal was measured in this case.

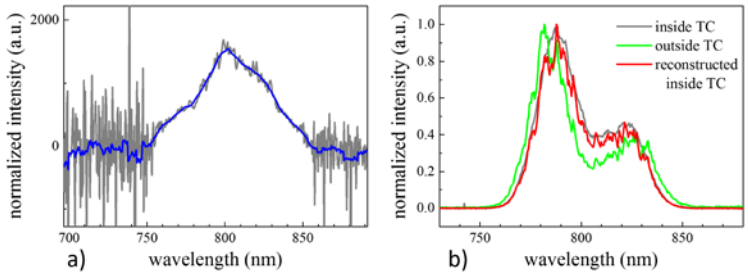

Fig. 2. a) Calibration factor in spectrum. The wavelength was smoothed with 20 points near each position. b) The reconstructed spectrum inside the chamber using a spectrum measured outside the chamber.

Additionally, to make sure that the measured back reflected light comes from the laser beam itself, rather than from plasma emission, the spectrum of the back reflected light was also calibrated by comparing the spectrum to laser radiation reflected from Al mirrors placed before the off-axis parabola [Fig. 2]. A spectral calibration curve was obtained through a 20-point smoothing at each position in the spectrum [Fig. 2(a)]. By using this calibration curve, the spectrum of back reflected radiation was reconstructed which proved to be the same as the incident beam spectrum, as depicted in Fig. 2(b). The energy and the spectrum of back reflected radiation were then monitored throughout the whole experiment.

3. Experimental and theoretical results

In the experiments, back reflected laser radiation from the target was measured when the laser pulse irradiated the target at an angle of incidence of 30°. In Fig. 3(a) the dependency of the measured back-reflection coefficient (reflected energy over incident energy) on laser intensity for target thicknesses 0.2 and 6 μm is shown. Over the intensity range investigated, the back reflection coefficient was in the range of a few %, and was seen to decrease with increasing laser intensity for the thinner targets (0.2 μm), while for the thicker targets (6 μm) the decrease was less pronounced. Overall, the back reflection coefficient was lower for the thinner target.

Optics EXPRESS

To understand these observations 2D PIC simulations (using the modified LSP code [18]) were performed, focusing on the characterization of the angular (spatial) characteristics of the reflected light from the target surface at oblique laser incidence on the target. In the simulations a p-polarized, 30 fs laser pulse with a Gaussian profile (temporal and spatial) is focused at intensity in the range 10^{18} - 10^{21} W/cm^2 in to a 4 μm spot on a Al^{+13} targets (0.2 and 2 μm) under 30 degree of incidence. The simulation box of 25 × 25 μm^2 contained 5000 × 5000 cells with 30 particles per cell. The density of electrons in the simulation boxes was set to 8 × 10^{23} cm^{-3}, which corresponds to the density of *Al* (2.7 g/cm^3) and a degree of ionization of + 13. The simulation starts at t = 0 when the laser pulse front (on the beam axis) is at 3 μm from the target surface.

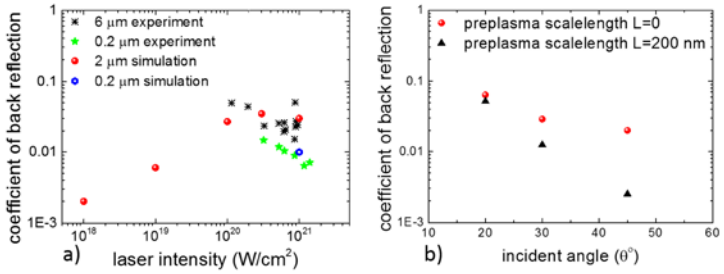

Fig. 3. a) Back reflection coefficient, measured from 0.2 μm and 6 μm *Al* targets and simulated, versus laser intensity. b) Dependence of the simulated back reflection coefficient on laser incidence angle on the target; the black triangles denote the results for preplasma scale length L = 200 nm and the red squares for L = 0 nm.

A substantial amount of back-reflected light was observed also in the simulation. It was seen that the back reflection coefficient increases with increasing laser intensity from 10^{18} W/cm^2 up to 10^{20} W/cm^2, reaching a reaching a peak at 3×10^{20} W/cm^2 [Fig. 3(a)]. The back reflection is substantially reduced if thin targets are used [at 0.2 μm in Fig. 3(a)]. The simulations also showed that the back reflected light increases significantly if the laser incidence angle on the target is decreased [Fig. 3(b)], as one would expect, given that the back reflection direction becomes closer to the specular direction. At oblique laser incidence the back reflection is sensitive to deformations of the target surface or to the presence of preplasma, - the back reflection could be reduced by introducing a small scale pre-plasma (L = 200 nm), compared to the case without pre-plasma (L = 0) in Fig. 3(b)). At 30° of incidence the presence of such a preplasma causes a decrease of the reflection coefficient by a factor ~3. However, the difference becomes insignificant for smaller angles of incidence.

We note that the contrast level of the laser systems prevents the formation of any significantly extended preplasma at the target surface. At the temporal contrast ~5×10^{-10} and laser intensity 10^{21} W/cm^2, the prepulse intensity will be ~5×10^{-11} W/cm^2 at a few ps before the main pulse. The temperature of the plasma at this intensity will be T< 100 eV [19]. Estimating for such temperature a velocity of the *Al* ions of about ~10^6 cm/s, the preplasma can only reach an extension of a few 10s of nm before the arrival of the main pulse, and essentially plays no role in the laser-target interaction.

A closer look to the dynamics of the interaction shows a significant distortion of the electron density profile and the presence of evolving structures on the target surface during the laser pulse [see Fig. 4 (a) and (b)]. The modification of the critical density surface starts already at a very early time [from 5.3 fs, Fig. 4(a)], and at the end of laser pulse a well defined, structured indentation on the target surface has been generated [Fig. 4(b)]. Regions within this structure, where the local normal is parallel to the laser axis result in the observed back reflection. The structure is formed due to the constant component of the force $\vec{F}_p = e[\vec{v}\times\vec{B}]/c$ (ponderomotive pressure), while the oscillating component of the $\vec{F}_p$ result in relativistic oscillations of the whole structure and the generation of attosecond pulses [8].

Optics EXPRESS

At even higher intensities this structure will lead to “hole boring”, where independently from the angle of incident on the target an electron density profile is formed which follows the spatial profile of the laser beam. In this case the reflection from the critical surface will mostly be directed backwards rather than in the specular direction determined by the original target surface. At intensities $\leq 10^{21}$ W/cm^2 an initial stage of “hole boring” is realized. The radiation pressure of the laser light curves the target critical density surface, enhancing the angular spreading of reflected light, so that reflection along the laser direction becomes possible.

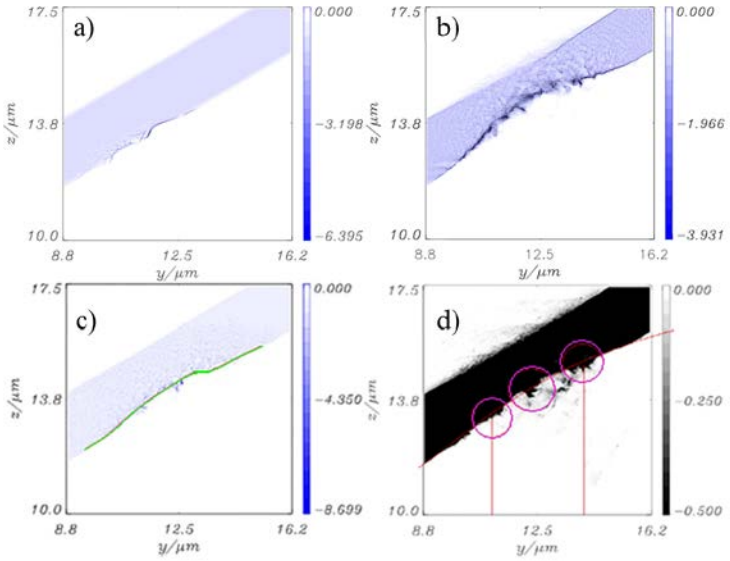

Fig. 4. Spatial distribution of the electron density profile on the target during the laser pulse at a) t = 5.3 fs, b) t = 32 fs and c) t = 21.3 fs from the start of the interaction for laser intensity 10^{21} W/cm^2. Colour scales are normalized on the initial electron density (8×10^{23} cm^{-3}), and it shown negative because it is electron charge density. d) t = 21.3 fs at the normalization of electron density to 3×10^{23} cm^{-3}.

The reflecting surface is curved as indicated in Fig. 4(c) at 21.3 fs from the start of interaction. The plot of Fig. 4(d) shows the same data but with a different color scale so that the profile for slightly lower target density can be visualized. Some structure can be visualized with areas where the surface normal is parallel to the incident beam axis. These electron density spikes oscillate and become a source for secondary waves, shown as circles in Fig. 4(d). Two spikes are at the edges of the laser pulse (shown with the vertical lines in Fig. 4(d)) and one close to the centre. The Figs. 4(b) and 4(d) are separated from each other by four laser periods but display the similar dynamic structure on the target surface. This suggests, that the structure of the electron density profile on the target surface is repeatable during the laser pulse.

The curvature of the reflecting surface of the target front and the spikes on it, shown in Fig. 4, are imprinted on the spatial profile of the reflected light. Figure 5(a) shows the distribution of the field at 42 fs, when the reflection of the pulse is finished. On Fig. 5(a) one of the constant phase surfaces of back reflected light is highlighted with red dots. The blue lines indicate two normals to these phase surfaces, whose intersection at the target surface indicates the “point”-like nature of the source of the reflected wave. For more precise identification of the location of the source of secondary waves a 2D electric field distribution map is shown in Fig. 5(b). The centers of the circles are the oscillating sources of secondary waves propagating also in backward direction. These centres correspond to the electron density spikes at the edges of the laser focal spot in Fig. 4(d). The secondary waves shown in

Optics EXPRESS

Fig. 5(b) as red circles coincide with the constant phase surface of the scattered light as one can see in simulations. The point source in Fig. 5(b) on the right side of the laser beam can be identified by the front of back reflected wave surface.

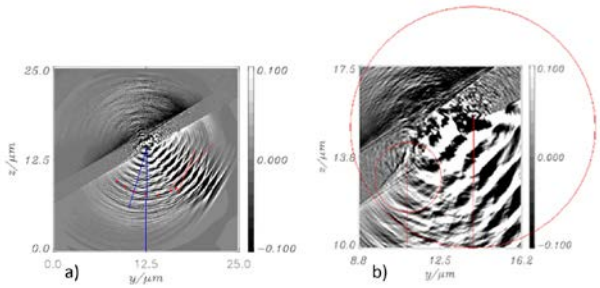

Fig. 5. a) 2D distribution of incident and reflected laser fields (E_y component) at 42 fs of laser interaction in the whole box of simulation. Scales are normalized to the incident laser amplitude. b) Zoomed 2D distribution of incident and reflected fields at 42 fs of laser interaction. The centers of spherical secondary waves are shown in c). Incident laser intensity is 10^{21} W/cm^2.

Clearly, in addition to the backscattering which was recorded by the detectors in the experiments there would be scattered light also under different angles. It is obvious from Fig. 5(a) that there are no point sources on the reflecting surface which are in phase. Thus, the source of backward emission (or reflection) will be the segments of electron densities oscillating with relativistic speed, and the reflected back radiation is effectively the diverging wave reflected from oscillating surface. The formation of such a structured density surface can be thought of as a "dynamical diffraction quasi-grating". A standard way of reconstructing the diffracted field from a conventional diffraction grating is to add the contribution of the wavelets originating from different parts of the grating, taking into account the phase differences between these sources of secondary emissions. In present case the sources of secondary emissions [Fig. 5(a)] are not stationary and they do not have strong regular distribution. Also, the observed quasi-grating, in contrast to conventional gratings has a range of spatial scales (fundamental and its harmonics) and formed by electron density profiles with different phase velocities. However, the distribution of point sources of secondary waves is not completely random. There are a number of articles devoted to the analysis of the plasma density profile formed through the development of various kinds of instabilities (Rayleigh-Taylor instabilities [20], two-stream instabilities [21], and generation of surface waves [22,23]), but we see the formation of quasi-periodic structures of the surface having certain (distinct) scale.

The diffraction pattern of the quasi-grating can be estimated for a fundamental harmonic with spatial period d and with phase velocity of the density profile v_{gr}. The angular distribution of the scattered radiation is described by the formula of moving grating with velocity v_{gr} in the lab reference frame with the reflection angle given by

$$\sin\theta_r = \frac{\sin\theta_i - n\lambda/d}{1 - \frac{v_{gr}}{c} n\lambda/d} \tag{1}$$

where n is the order of diffraction, θ_r and θ_i are the angles of reflection and incidence, respectively. We should mention that use of Eq. (1) to interpret the scattered field from the profile shown in Fig. 4(d) is an approximation, as the "quasi-grating" on Fig. 4(d) consists of only a few spikes which are generating secondary spherical waves.

From Eq. (1) it follows that at $v_{gr} = c/\sin\theta_i$ there will be only specular reflection ($\theta_r = \theta_i$) at any grating constant. This is the case for non-relativistic laser amplitude. However, the simulation shows, that $v_{gr} < c/\sin\theta_i$ which is due to the nonlinearity and the inertia of the

Optics EXPRESS

electron motion in the relativistic field. For high amplitude oscillations, the electrons cannot follow the oscillations of the electric field and $\vec{F}_p$. At relativistic intensities (10^{21} W/cm^2 in our case) the electron and electromagnetic waves are therefore not in phase. The trajectories of the electrons are more complex than simple oscillations around the surface. The electric field has a component along the target surface and forces the electrons to move back and forth along the surface. At relativistic intensities, $\vec{F}_p = e[\vec{v} \times \vec{B}]/c$ is of the same order as the force of the electric field and breaks the symmetry of the oscillations. In average a compensation of the force $\vec{F}_p$ by an ambipolar field takes place in time, but the instantaneous phase of the electron oscillations will differ from the phase of the incident field, because at high amplitudes of oscillations and relativistic mass the electrons cannot follow the changes in the field phase. Another cause of dephasing of the electron oscillations with respect to the laser field is the specular reflection of the laser light which pulls out the electrons from the target surface (due to the strong field gradients with spatial scales shorter than the laser wavelength), resulting in the formation of additional spikes in the electron density. Therefore, due to the laser ponderomotive pressure the distance between the spikes and their profile does not correspond to the period of the incident laser beam because of the nonlinear motion of electrons in the relativistic field.

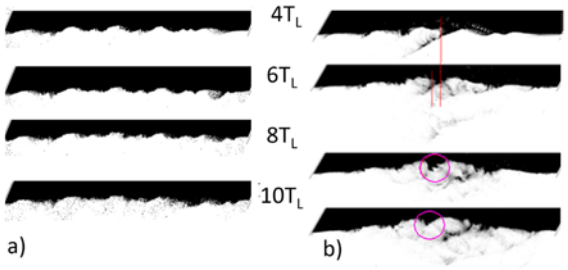

Fig. 6. The electron density profiles are depicted for integer number of laser periods: $4T_L$, $6T_L$, $8T_L$, $10T_L$ for laser intensities a)10^{19} W/cm^2 and b) 10^{21} W/cm^2. Pulse duration 30 fs, 30° incidence, at the beam diameter 4 μm, size on the target 8.5 μm.

In Fig. 6 the electron density profiles are depicted for integer number of laser periods:,, $4T_L$, $6T_L$, $8T_L$, and $10T_L$ for laser intensities 10^{19} W/cm^2 and 10^{21} W/cm^2. In Fig. 6a) besides modulations with periodicity $d = \lambda/\sin\theta$ we see harmonics of $d \sim \lambda/\sin\theta$ (due to the force $\vec{F}_p = e[\vec{v} \times \vec{B}]/c$) and even more complicated structure resulting from two phase-shifted, overlapped gratings (incident field relative to reflected).

The specularly reflected light has the same front velocity $c/\sin\theta$ relative to the target front while the electron bunches are moving along the target surface with velocity ~c and have a velocity component $c/\sin\theta$ on the target surface. The appearance of the velocity $c/\sin\theta$ leads to a delay between the velocity spike and the peak of the incident laser field pulling the electrons out of the surface.

On Fig. 6(b) the gap between the red lines indicates the phase shift between the incident wave and the response of the electron density spike. We emphasize that we have described the effects which are associated with ultrahigh intensities and disappear in a linear mode of interaction. Comparison of Figs. 6(a) and 6(b) shows that the surface profiles are substantially different for different intensities (and basic harmonics of modulation period $\lambda/\sin\theta$). These observations and the results of calculations [see. Figure 5] suggest that $v_{gr} < c/\sin\theta_i$. In Fig. 5 (a) and (b) this is confirmed by the secondary spherical waves emitted from the surface. At $v_{gr} < c/\sin\theta_i$ such waves should not occur in spite of the complicated structure of target surface.

The Eq. (1), for the fundamental harmonics (oscillations caused by tangential component of the electric field) of the grating period $d = \lambda/\sin\theta$ gives the diffraction peak of second order ($n = 2$) in the backward direction for speed $v_{gr} \ll c$. For the harmonics with grating constant

Optics EXPRESS

$d = \lambda/2\sin\theta$ (caused by oscillations of $\vec{F}_p$), the diffraction maximum in the backward directions will be in the first order (n=1) at $v_{gr} \ll c$.

We emphasize that the low "quality" of the quasi-grating results in a significant blurring of the angular peaks. If one looks at Fig. 5(a) in terms of "diffraction" pattern, then besides the specular maxima (n = 0) two additional angular peaks can be identified close to the blue straight lines. Reducing the laser intensity the role of non-linear effects is weakening and in the experiments and PIC simulations we see a decrease of scattered light under different angles and scattering only in the specular direction remains.

In average at intensities 10^{20} – 10^{21} W/cm^2 the amplitude of back reflection is about 3% of the amplitude of incident beam. Shortening of the wavelength of back reflected light due to the movement of reflecting surface (Doppler effect) were evaluated in [19,24]. At higher intensities (10^{21} W/cm^2) and thin targets the structure of the reflecting surface will become more chaotic resulting in more diffused reflection and in the decrease of the reflection coefficient. The structure formed on the target surface becomes comparable to the target thickness, and the back reflection is reduced. We are observing a tendency of decreasing coefficient of back reflection for thin targets (0.2 μm) with increasing laser intensity for the same reason.

The measured coefficient of back reflection agrees well with the PIC simulation as shown in Fig. 2(a). Both experiments and simulation do not show a strong dependence from laser intensity in the range 10^{20} – 10^{21}W/cm^2. The spread of experimental data is related to the transient nature of the processes which are intrinsically not stable. Simulations show, that with decreasing the laser intensity the coefficient of back reflection is decreasing because the generated structure on the target surface will be suppressed. Therefore, there is a maximum in the coefficient of back reflection dependent on laser intensity.

Now it becomes clear that the observed reduction of back reflection by introducing a small pre-plasma [200 nm in Fig. 2(b)] is a result of the suppressed regular structure on the target surface due to pre-plasma. The back reflection is seen to decrease much faster for increasing incidence angle if there is a pre-plasma compared to the case with no preplasma. However, the difference is diminishing when laser incident angle tend to normal.

4. Conclusion

To summarise, we report a finding of high relevance to the ongoing development of laser technology towards the multi-PW power level. We have demonstrated by PIC simulations the dynamics of the generation of regular structures in the electron density profile at the laser-target interface during PW, ultrashort laser pulse interaction with a solid target. This structure can act as a quasi-grating and, as a result, a significant amount of laser energy can be reflected back into the beam transport system, as observed experimentally. Additionally, we have demonstrated in PIC simulations that with a small amount of pre-plasma at the target front this regular structure is smeared out and the back reflection reduced.

The observed phenomena can have serious consequences when using PW laser systems in the interaction experiments. In laser-solid interaction experiments, the dynamics and the properties of the target surface can result in significant amount of reflected back laser light not only in form of laser harmonics but also on the fundamental frequency which can be "re-collimated" by the focusing parabolic mirror and propagate back into the laser chain. This back-reflected light with the same wavelength and energy content of the order of 1% of the incident laser energy can effectively travel back along the laser system and can cause serious damage due to imperfect collimation, which may be focused on optical components in the laser chain.

Funding

Institute for Basic Science (IBS) (IBS-R012-D1); EPSRC (EP/K022415/1, EP/J500094/1).